We are IntechOpen, the world's leading publisher of Open Access books Built by scientists, for scientists

4,800
Open access books available

122,000
International authors and editors

135M
Downloads

Our authors are among the

154
Countries delivered to

TOP 1%
most cited scientists

12.2%
Contributors from top 500 universities

CLARIVATE ANALYTICS BOOK CITATION INDEX INDEXED

WEB OF SCIENCE™

Selection of our books indexed in the Book Citation Index in Web of Science™ Core Collection (BKCI)

Interested in publishing with us?
Contact book.department@intechopen.com

Numbers displayed above are based on latest data collected.
For more information visit www.intechopen.com

17

Novel Deposition Technique for Fast Growth of Hydrogenated Microcrystalline Silicon Thin-Film for Thin-Film Silicon Solar Cells

Jhantu Kumar Saha[1,2] and Hajime Shirai[1]
[1]*Department of Functional Material Science & Engineering, Faculty of Engineering, Saitama University,*
[2]*Current address: Advanced Photovoltaics and Devices,(APD) Group, Edward S. Rogers Sr. Department of Electrical and Computer Engineering, University of Toronto,*
[1]*Japan*
[2]*Canada*

1. Introduction

The microcrystalline silicon material is reported to be a quite complex material consisting of an amorphous matrix with embedded crystallites plus grain boundaries. Although this material has a complex microstructure, its optical properties have a marked crystalline characteristic: an optical gap at 1.12 eV like c-Si. This implies the spectral absorption of μc-Si:H covers a much larger range than a-Si:H which posses an optical gap between 1.6 and 1.75eV[i]. Compared to a-Si:H that absorbs light up to 800 nm, μc-Si:H absorbs light coming from a wider spectral range, extending up to 1100 nm . On the other hand, within its range of absorption, the absorption of a-Si:H is higher than that of μc-Si:H –due to the indirect gap of the latter. Therefore, the optical combination of these two materials takes advantage of a larger part of the solar spectrum (compared to a single-junction cell) and the conversion efficiency of the incident light into electricity can be consequently improved. Furthermore, the μc-Si:H solar cell is reported to be largely stable against light induced degradation and enhanced carrier mobility in contrast to amorphous silicon films counterpart. Consequently hydrogenated microcrystalline silicon is one of the promising materials for application to thin-film silicon solar cells.

2. Growth techniques of hydrogenated microcrystalline silicon

The growth of μc-Si:H material uses silane (SiH_4) and hydrogen as source-gas. It is currently admitted that free radical precursors (SiH_x)-SiH_3 is suspected to favor the μc-Si:H growth- and H-enhances crystalline growth by etching of looser a-Si:H tissue-were needed to attain microcrystalline growth. In order to obtain such reactive species, decomposition of the source-gases is necessary. At first, this was obtained by using PE-CVD at high temperatures (600˚C). The use of low deposition temperatures of 200-300˚C with a plasma present in the

deposition chamber, the so called Plasma-Enhanced Chemical Vapor Deposition technique (PE-CVD) was developed later on and allowed the low-temperature deposition of μc-Si:H films, and rapid progresses have been achieved. Unfortunately, "state-of-the-art" microcrystalline silicon solar cells consist of intrinsic μc-Si:H layers that are deposited by rf and VHF PE-CVD at deposition rates of only 1-5 Å/s. On the other hand, a μc-Si:H film with a 2-μm- thickness intrinsic absorption layer is required for application to Si thin-film solar cells because of the low optical absorption in the visible region. The μc-Si:H i-layer deposition step is the most time consuming step in the deposition sequence of the solar cell. Therefore, a novel fast deposition technique of μc-Si:H is required.

3. Novel fast deposition techniques of microcrystalline silicon

Now-a- days, for the high throughput of high-efficiency μc-Si solar cells in PV industry, one of the most crucial requirements is fast deposition of μc-Si without deteriorating the optical, structural and electronic properties of the film. To overcome the difficulty, several high-density plasma sources have been developed, such as very high frequency (VHF) plasma, inductive coupling plasma (ICP) and surface wave plasma (SWP). As it has been reported, the excitation frequency of a plasma source has an important effect on the electron acceleration in the plasma, and a high excitation frequency is expected to result in a high electron density and a low electron temperature. Therefore two new microwave plasma sources have been developed i.e. Low-pressure high-density microwave plasma source utilizing the spoke antenna and the remote-type high-pressure microwave plasma using a quartz tube having an inner diameter of 10 mm and applied those for the fast deposition of μc-Si films for Si thin-film solar cells. The remote-type high-pressure microwave plasma will be discussed in elsewhere.

3.1 Low-pressure high-density microwave plasma source utilizing the spoke antenna

The microwave plasma source is shown schematically in Fig. 1, which is composed of the combination of a conventional microwave discharge and a spoke antenna. Its chamber size is 22 cm in diameter, which enables large-scale film processing. The spoke antenna is located on a 15 mm-thick quartz plate, which is not inside of the vacuum chamber. The antenna system is shown in Fig. 2 more in detail. The length of each spoke is 4 cm, which is about 1/4 of the wavelength of a 2.45 GHz wave. The design of the spoke antenna assembly

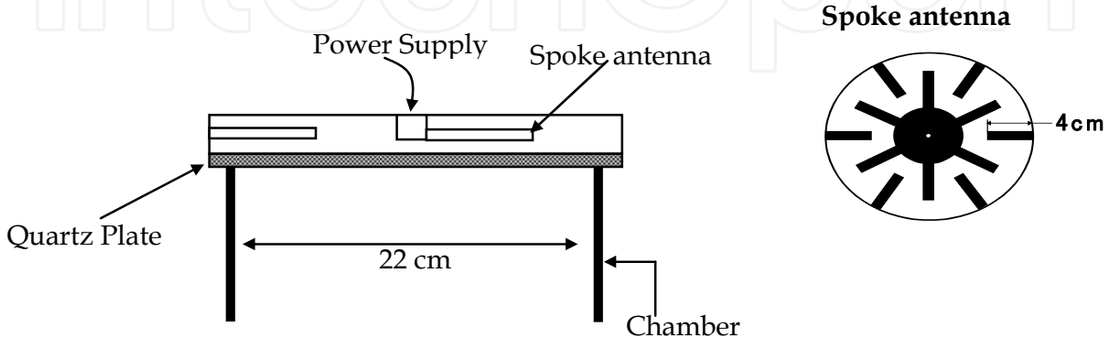

Fig. 1. A schematic illustration of the microwave plasma source

is based on an inter-digital filter composed of parallel cylindrical rods (spokes) arranged between parallel-grounded plates. The spokes are resonantly coupled by the stray capacitance between adjacent spokes and the inductance of the spokes themselves. The resonance condition of an introduced angular frequency is given by $\omega=2\pi f=1/(C\times L)^{1/2}$, where f is the introduced frequency, C is the array capacitance, and L is the antenna inductance. Thus, the antenna operates as a band-pass filter. The spokes are arranged like those in a wheel, and the plasma serves as one of the grounded plates. The electromagnetic wave propagates through the spokes consecutively with a phase difference of 90°, and microwave current flows in every spoke. The current in the spokes couples inductively and capacitively to the plasma ("CM coupling"), and the induction current in the plasma accelerates the electrons to sustain the plasma, as shown in Fig. 2 & 3. The power is supplied from the center of the antenna, and the plasma under the spoke antenna is radially discharged because induction current flows near every spoke. As a result, uniform microwave plasma over an area of diameter greater than 20 cm can be generated efficiently. As well, since no magnetic field is required to generate the high-density microwave plasma, it is possible to design a simple source yielding high-density and low-temperature plasma.

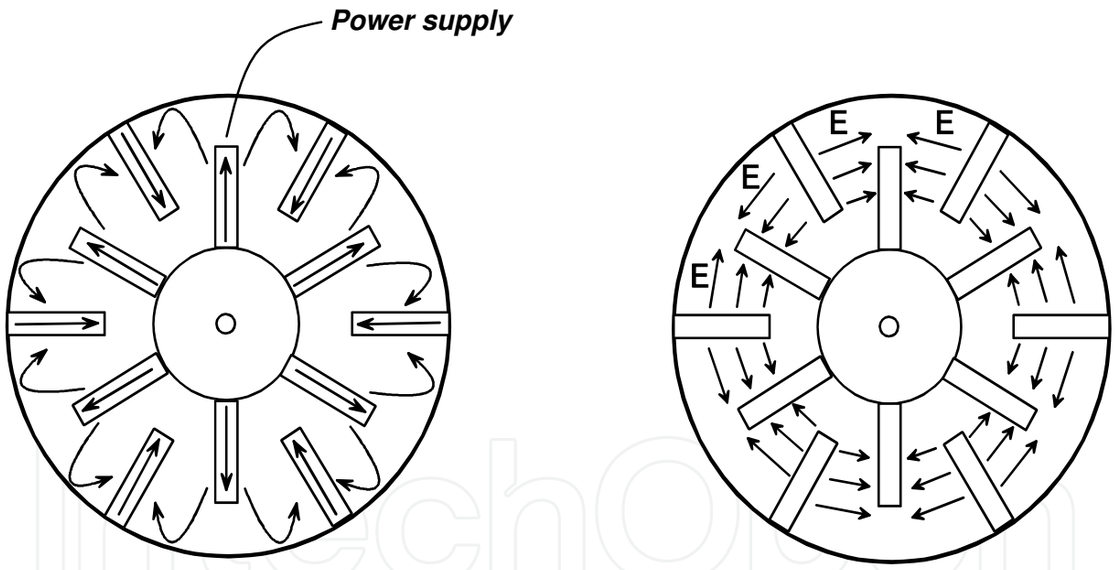

(a) Microwave current (b) Electric field

Fig. 2. The newly developed spoke antenna for introduction of microwave power (a) Microwave current, (b) Electric field.

From a material processing standpoint, large-area microwave plasmas (MWPs) have several advantages in comparison with other types of high-density sources. First, MWPs, being no magnetized sources, are free from such magnetic field induced problems as inhomogeneous density profile and charge-up damage, which is often, experienced in electron cyclotron resonance (ECR) or helicon plasma sources. Second, MWPs can be enlarged to diameters

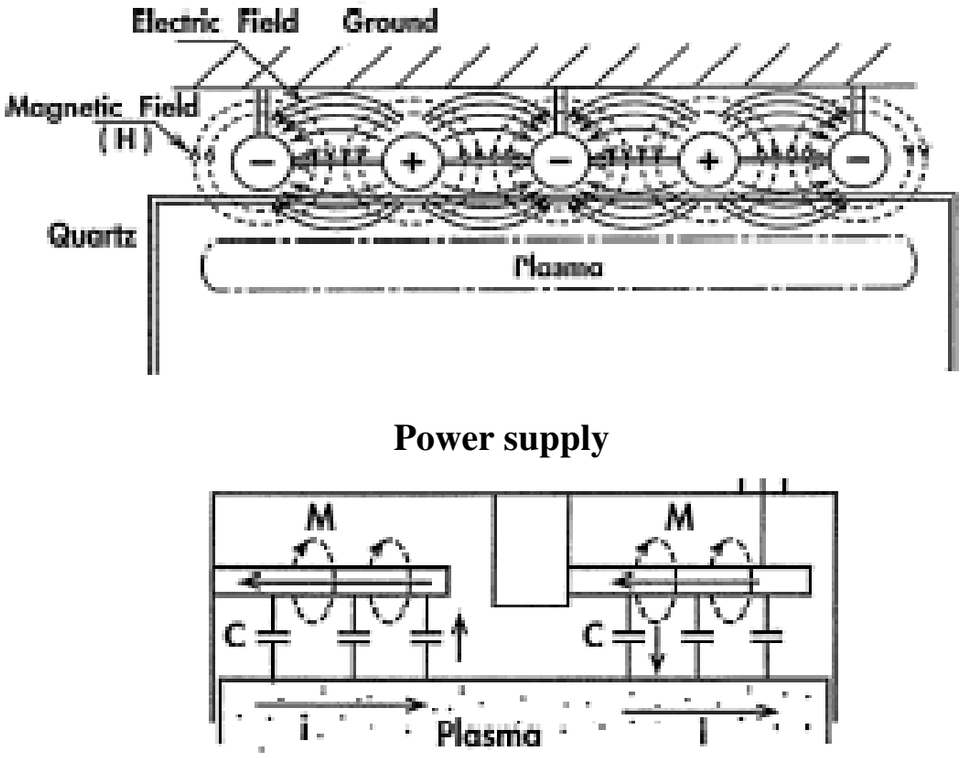

Fig. 3. The coupling of the spoke antenna with microwave plasma [x]

(a) (b)

Fig. 4. Images of Ar plasma at a) 80 mTorr and b) 20 Torr. The plasma maintains uniform state under a wide pressure regime.

longer than 1 m more easily than inductively coupled plasmas (ICPs). Thus, the application of MWPs to giant electronic devices such as solar cells is promising. Third, MWPs have lower bulk-electron temperature. Fourth, MWPs can be operated stably from atomic pressure down to below 10 mTorr. Fig. 4. demonstrates that Ar plasma maintains a uniform state over 22 cm in diameter up to 20 Torr. The schematic diagram of the low-pressure high-density microwave plasma utilizing the spoke antenna is shown in Fig. 5.

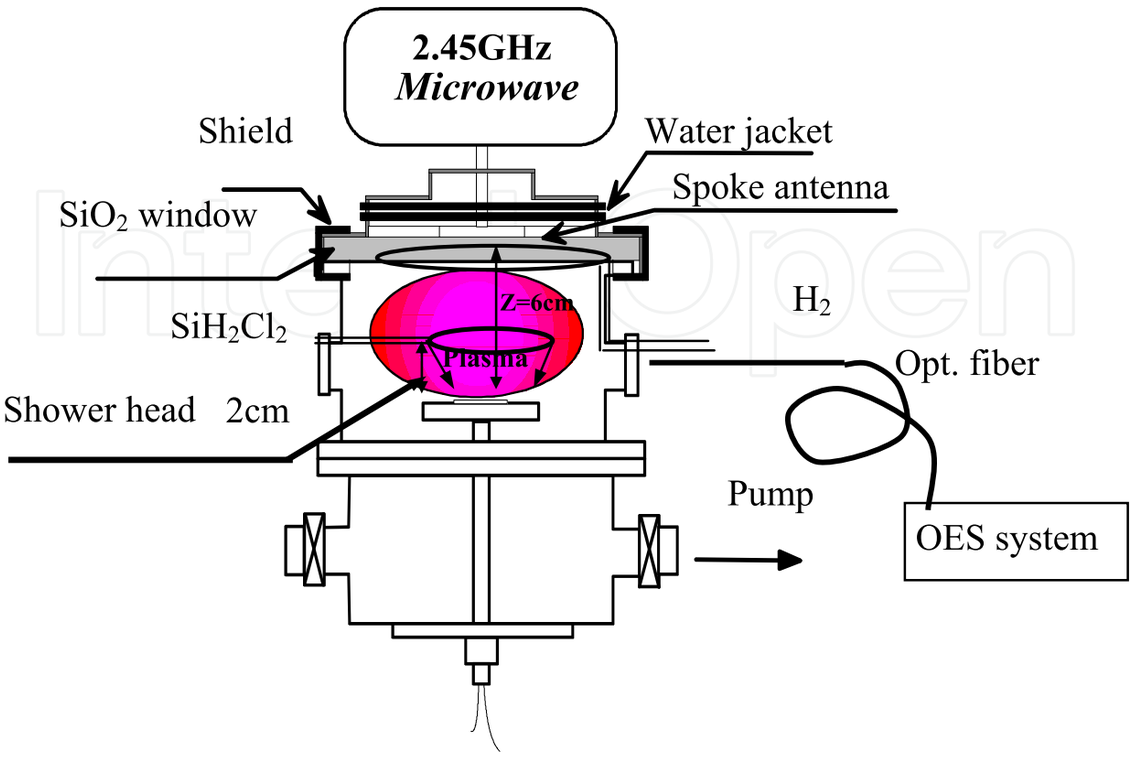

Fig. 5. The schematic diagram of the low-pressure high-density microwave plasma utilizing the spoke antenna

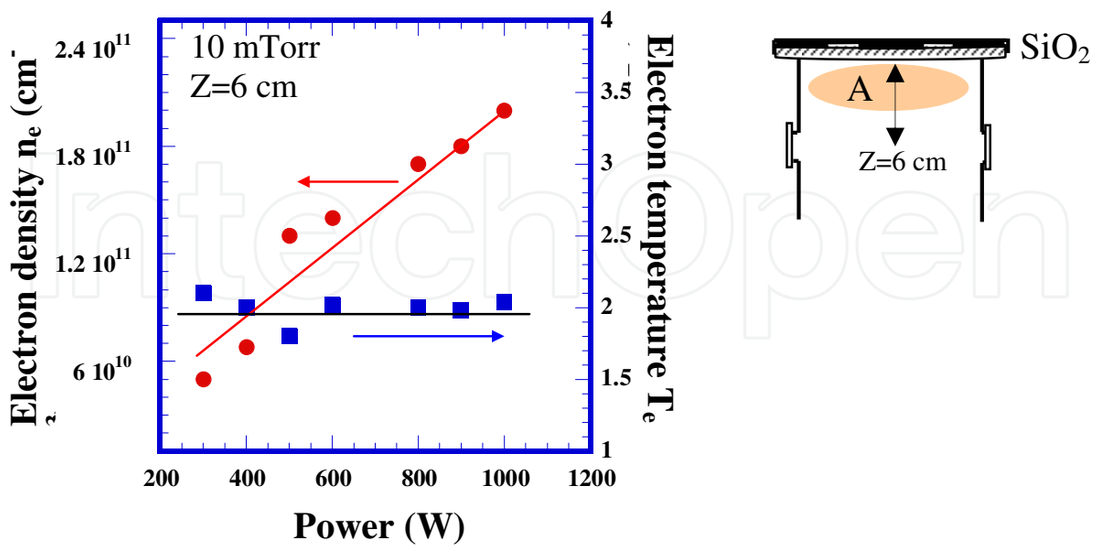

Fig. 6. Electron density, n_e, and electron temperature, T_e, measured as a function of input microwave power.

A uniform, high-density (electron density, n_e: >10^{11} cm^{-3}) and low-temperature (electron temperature, T_e:1~2 eV) plasma can be generated by the microwave plasma source utilizing a spoke antenna without using complex components such as magnetic coil as shown in Figures 6 & 7 . The T_e is almost independent of working pressure up to ~150 mTorr as shown Figure 8, which is suitable for the large area thin film processing.

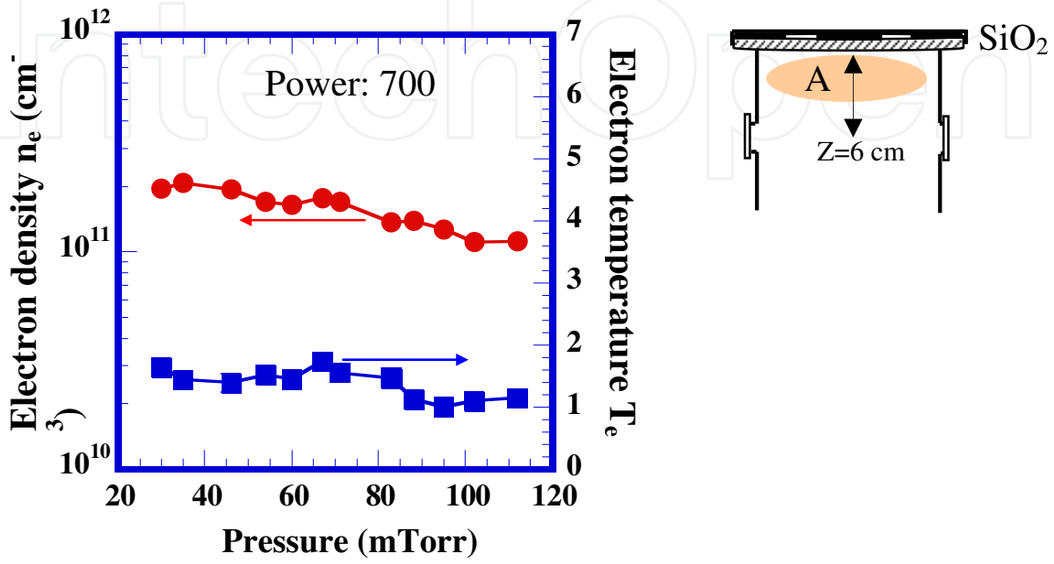

Fig. 7. Electron density and electron temperature plotted against working pressure.

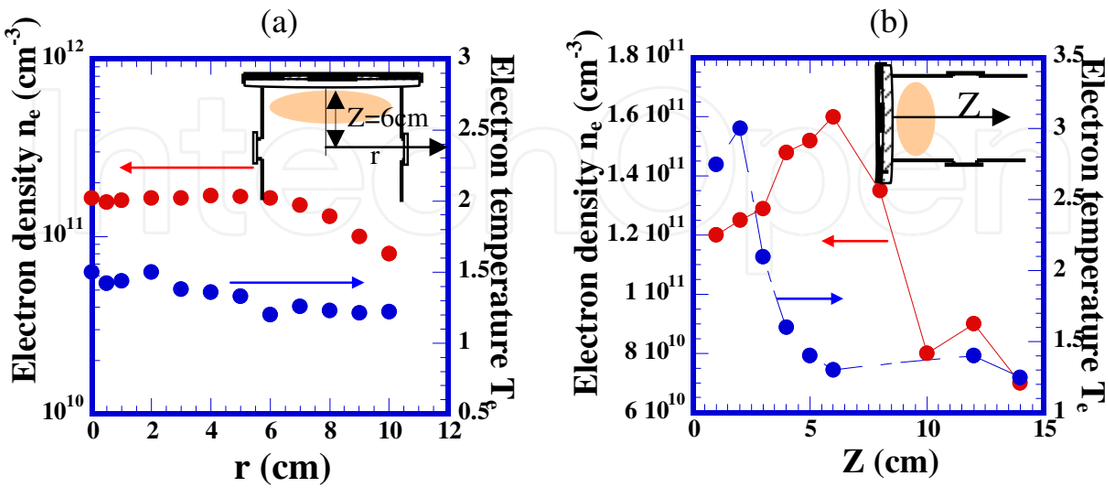

Fig. 8. The radial and axial distributions of n_e and T_e in microwave Ar plasma under microwave power of 700 W at 80 mTorr with Ar flow rate of 20 sccm.

3.2 Fast deposition of highly crystallized μc-Si:H films with low defect density from SiH_4 using low-pressure high-density microwave plasma

In this study, a new source gas supply method was introduced, i.e., the SiH_4 was introduced using a shower head placed 2 cm above the substrate holder under a steady flow of the H_2 plasma supplied by the ring. The results from these gas supply method were compared with the results from the another gas supply method, i.e. a SiH_4-H_2 mixture was fed into the chamber using a ring just beneath the quartz plate. Figure 9 shows the schematic of the two different gas supply methods. The film deposition parameters were included the SiH_4 concentration $R=Fr(SiH_4)/[Fr(SiH_4)+Fr(H_2)]$ (Fr is the flow rate). The SiH_4 concentration was varied in a range from 5% to 67% by increasing $Fr(SiH_4)$ from 3 to 30 sccm with a constant H_2 flow rate of 15 sccm. The film depositions were performed at the distance (Z) between the quartz plate and the substrate holder of 6 cm and the working pressure of 80 mTorr. The microwave power was fixed at 700W.

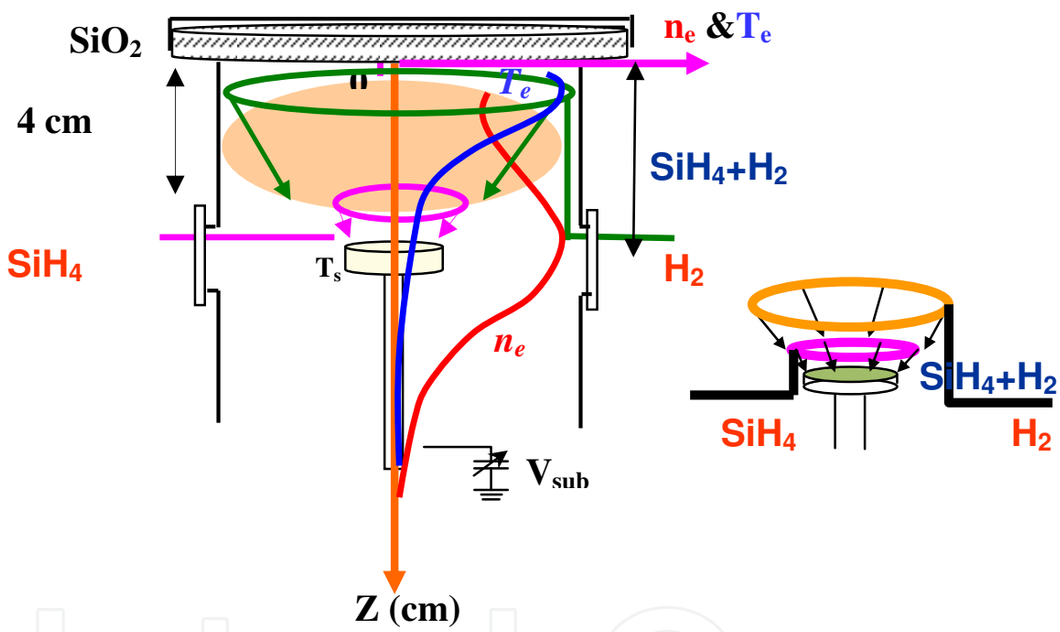

Fig. 9. Schematic of the two different gas supply methods used in this study. The distance (Z) between the quartz plate and substrate holder was 6 cm.

Fig. 10 shows the deposition rate dependence of ESR spin density, N_s for the corresponding μc-Si films fabricated using two different SiH_4 gas supply methods at T_s of 150 and 250°C. Here, the film deposition rate was controlled by varying $Fr(SiH_4)$ from 3 to 30 sccm under constant $Fr(H_2)$ of 15 sccm and working pressure of 80 mTorr. For all samples, the film thickness was ~ 1.5 μm and the ESR measurements were performed directly on these films. It is to be noted that N_s was decreased by about one order of magnitude when the shower head was used for both T_s conditions despite the other deposition conditions being the same. However, N_s was almost independent of $Fr(SiH_4)$ on the order of $(3\text{-}4)\times10^{16}$ cm^{-3}, which was still one order of magnitude larger than that of high quality μc-Si films reported elsewhere.

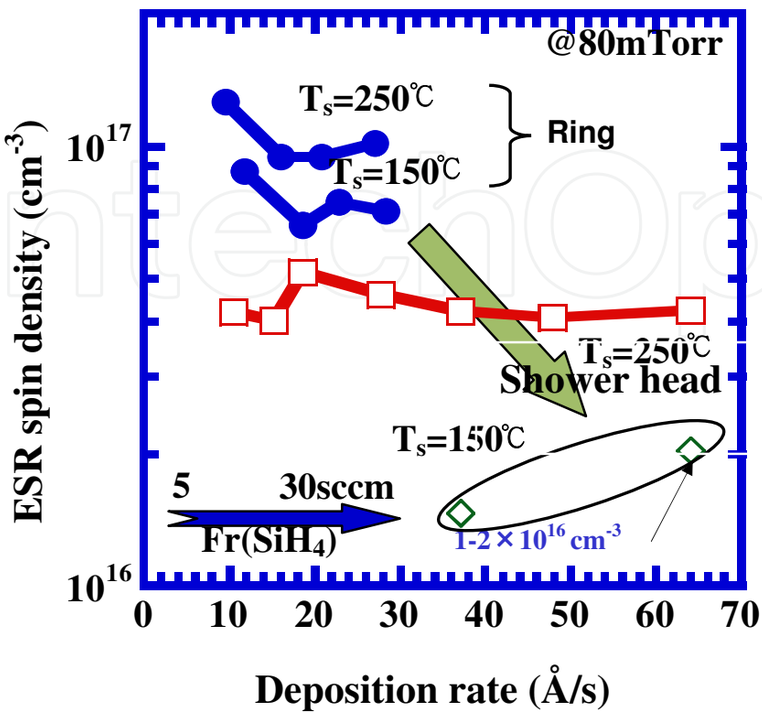

Fig. 10. ESR spin density, N_s for corresponding μc-Si films fabricated using different gas supply method as well as that for samples prepared at T_s=150˚C are plotted as a function of film deposition rate R_d.

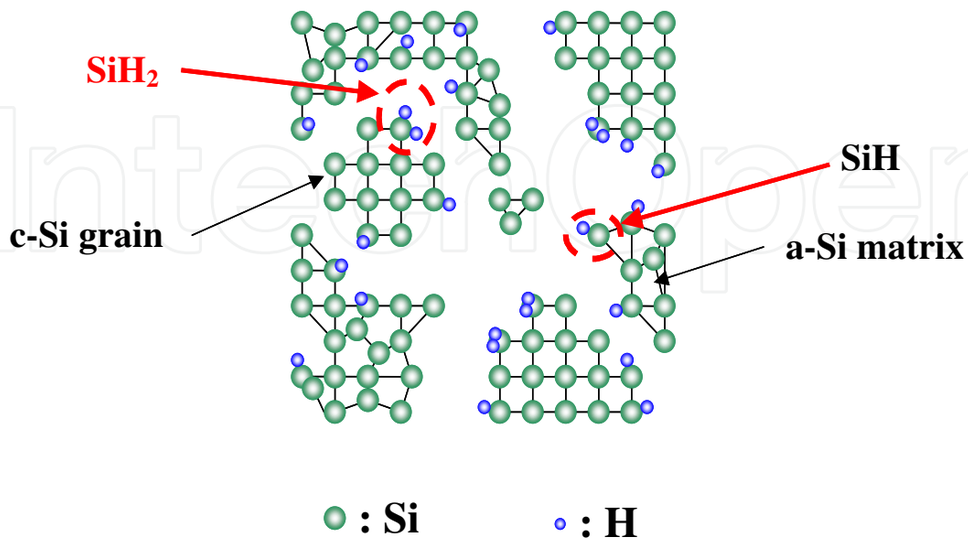

Fig. 11. μc-Si:H film microstructure

A very fast deposition rate of 65Å/s has been realized for μc-Si:H films with a Raman crystallinity ratio of Ic/Ia of about 3.5 under very low H_2 dilution (i.e. with high SiH4 concentration of 67%) as shown in Fig. 12 and low defect density of (1-2) $\times 10^{16}$ cm^{-3} using high-density and low-temperature microwave plasma. The imaginary part of the dielectric function $\langle \varepsilon_2 \rangle$ spectra of μc-Si:H films fabricated from SiH_4 using high-density and low-temperature microwave plasma is shown in Fig. 13 along with that using rf PE-CVD methods. Using the optical model the best fitted volume fraction of c-Si and void i.e. *f*c-Si and *f*void in the bulk layer and void in surface layer, f_{void}, with SiH_4 concentration R for the corresponding μc-Si films is shown in Fig. 14.

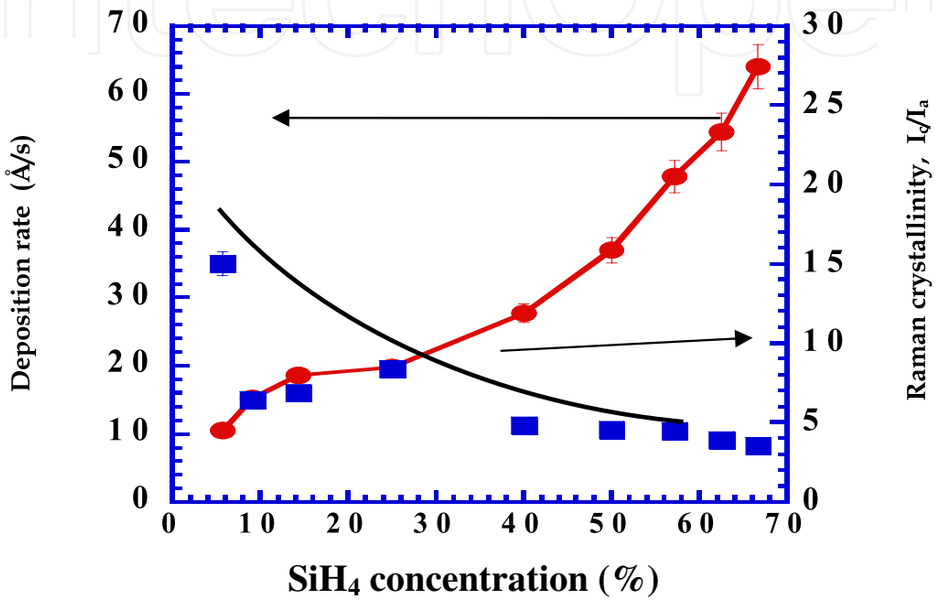

Fig. 12. Film deposition rate and Raman crystallinity, I_c/I_a as a function of SiH_4 concentration R: $Fr(SiH_4)/Fr(SiH_4)+Fr(H_2)$.

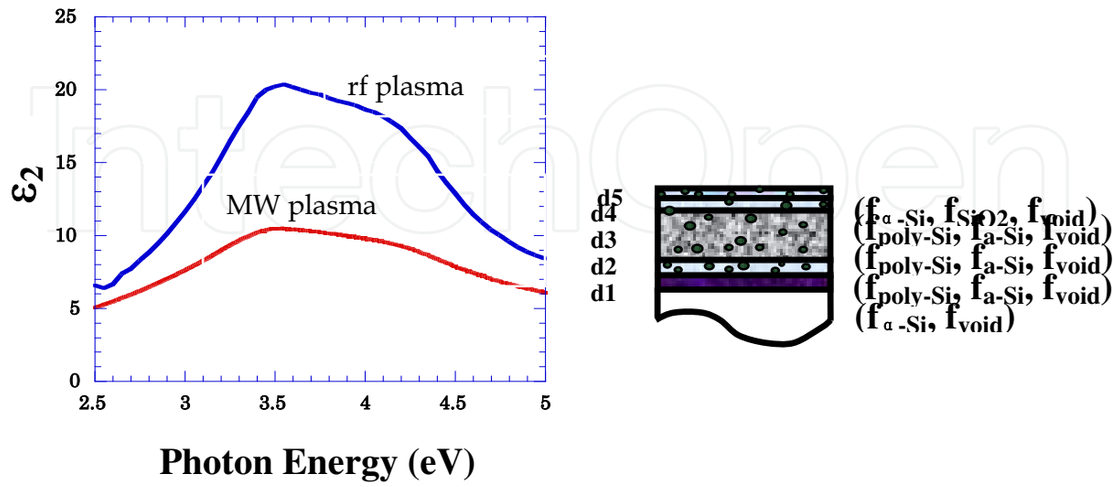

Fig. 13. Imaginary part of the pseudo dielectric function$\langle \varepsilon_2 \rangle$ spectra for the μc-Si films fabricated from SiH_4 using MW Plasma along with that using rf PECVD methods and five layers optical model.

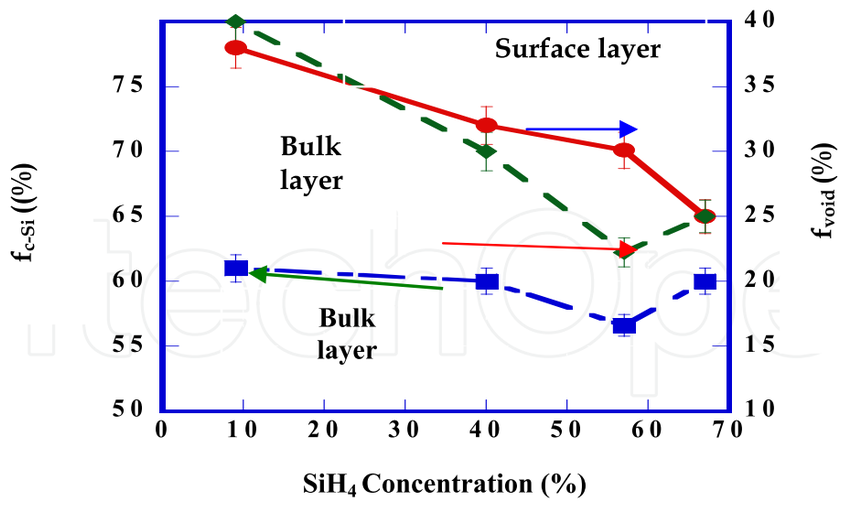

Fig. 14. Changes in $f_{c\text{-}Si}$ and f_{void} in the bulk layer and surface layer, with SiH_4 concentration R for the corresponding μc-Si films shown in Fig. 11.

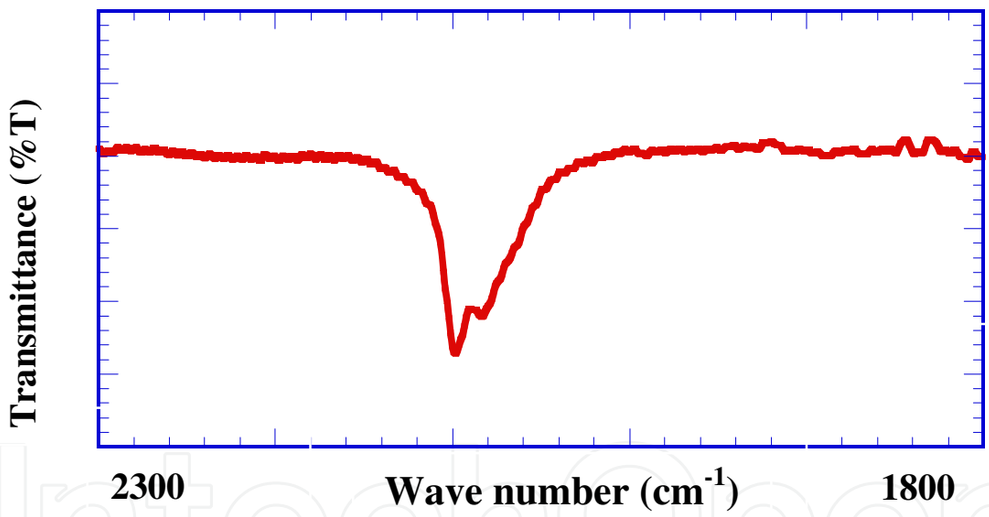

Fig. 15. The FTIR spectra for the corresponding μc-Si:H films fabricated from SiH_4 using MW plasma.

Highly crystallized μc-Si:H film was synthesized despite low H_2 dilution ratio rather than the conventional rf and VHF plasmas, because of high generation efficiency of atomic hydrogen. FTIR spectra and microstructure of μc-Si:H film and of SiH_n absorption region are shown in Fig. 11 & 15 for the corresponding μc-Si film. Generally, two IR absorption peaks are observed at 2000 and 2100 cm^{-1}, which are attributed to the bulk SiH in a-Si and SiH_2 in μc-Si phase, respectively, in the film fabricated by the rf plasma CVD. However, no SiH absorption peak at 2000 cm^{-1} is observed in the film fabricated by high-density microwave plasma. These imply that the film crystallization is promoted extremely in the high-density plasma with negligibly small fraction of amorphous Si phase. In addition, the

IR absorption peak at 2090 cm^{-1} corresponding to the surface SiH mode in the μc-Si phase appeared as a shoulder in the high-density film. These results suggest that the c-Si phase is isolated in a-Si network as shown in Fig. 11 & 16, which is not preferable for the Si thin-film solar cells. Therefore, the suppression of the excess film crystallization is required by the selection of deposition precursor.

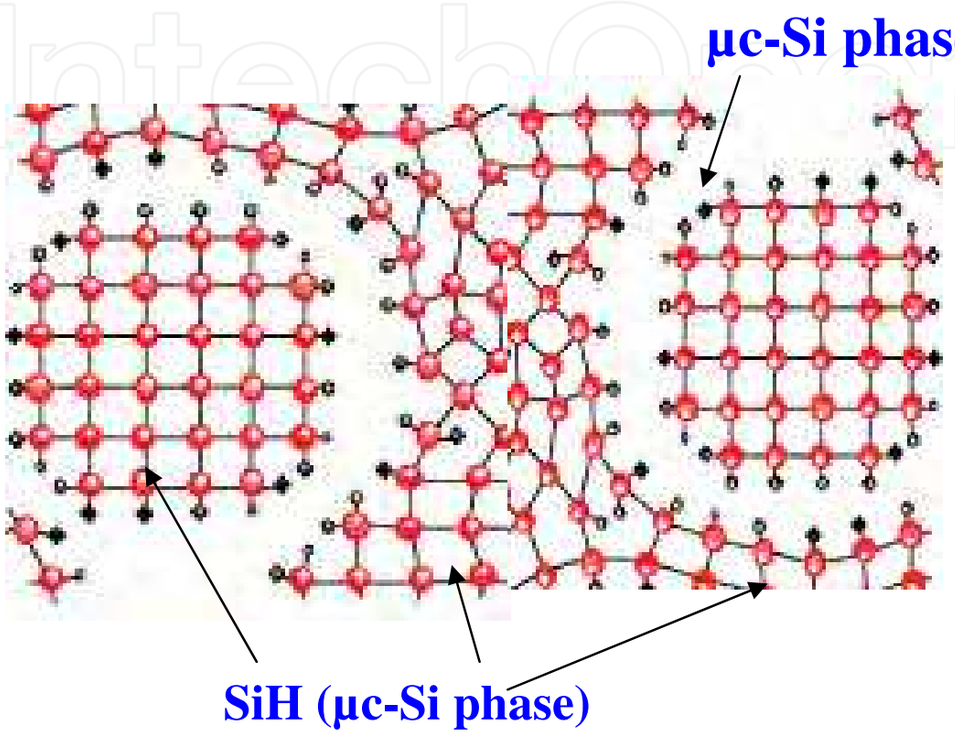

Fig. 16. μc-Si:H films fabricated from SiH_4 using MW plasma

Highly crystallized μc-Si:H films with a preferred (220) crystal orientation at a high deposition rate of 65 Å/s were fabricated from SiH_4 with a negligibly small volume fraction of amorphous Si but μc-Si network included high volume fraction of voids as shown in Fig. 15. which was hardly compatible with a device quality material. To overcome this problems, the fast deposition of highly photoconductive hydrogenated chlorinated microcrystalline Si (μc-Si:H:Cl) films with amorphous Si phase and with less volume fraction of void have been fabricated from SiH_2Cl_2 with higher threshold energy for the dissociation instead of SiH_4.

3.3 Fast deposition of highly crystallized μc-Si:H:Cl films with low defect density from SiH_2Cl_2 using low-pressure high-density microwave plasma

3.3.1 Fine structure of Si network of microcrystalline silicon thin-film fabricated from SiH_2Cl_2 and SiH_4

The typical FTIR spectra of 1-μm-thick μc-Si:H:Cl films fabricated from a SiH_2Cl_2-H_2 mixture, compared with those of μc-Si:H films from SiH_4 as shown in Fig. 17. Here, the peak assignments of SiH (bulk and surface stretching) and SiH_2 bulk stretching are also shown in Table 1.

Si-H (bulk stretching)	**2000 cm^{-1}**
Si-H (surface stretching)	**2080 cm^{-1}**
SiH_2 (bulk stretching)	**2100 cm^{-1}**

Table 1. Assignment of SiH, SiH_2 vibration modes

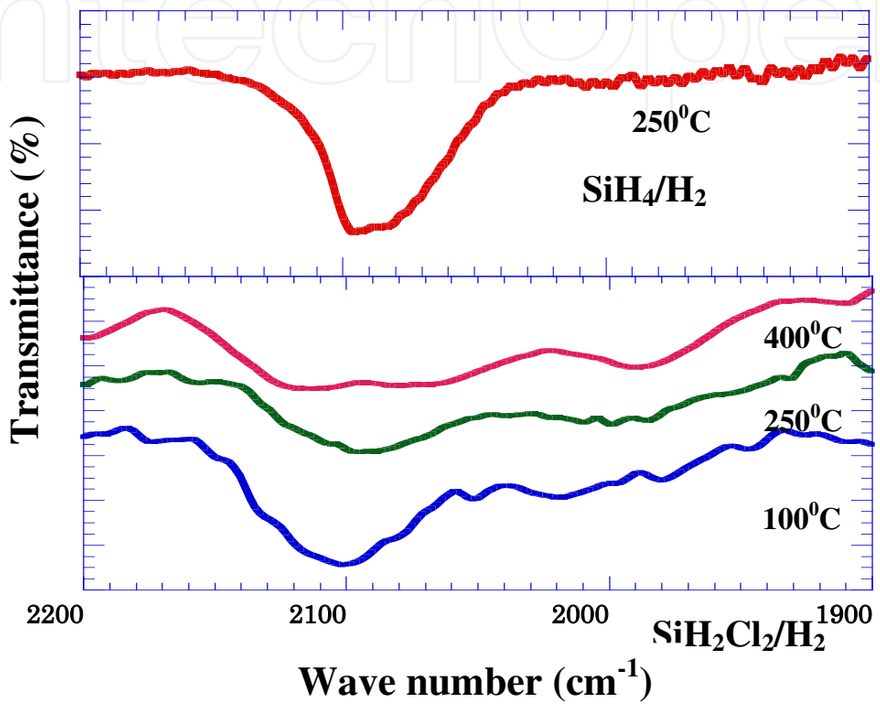

Fig. 17. FTIR spectra of µc-Si:H:Cl films at different T_ss. The typical FTIR Spectrum for the SiH_x stretching absorption region in the µc- Si:H film from SiH_4 is also shown as a reference.

However, marked differences were observed in the fine structure between µc-Si:H:Cl and µc-Si:H. In the µc-Si:H films from SiH_4, the absorption peaks at 2080 cm^{-1} and 2100 cm^{-1} attributable to surface and bulk SiH_x stretching absorption modes, respectively, in the nanocrystalline Si phase were dominant with a negligibly small peak of SiH absorption in the bulk a-Si phase at 2000 cm^{-1}. Thus, the film is highly crystallized with a negligibly small fraction of the amorphous Si phase. In addition, the IR absorption peak at 2080cm^{-1} corresponding to the surface SiH mode in the µc-Si phase appeared as a shoulder in the µc-Si:H film. These results suggest that the c-Si phase is isolated in a-Si network, which is not preferable for the Si thin-film solar cells. Moreover, because of excess dissociation of SiH_4, the µc-Si:H network showed a porous structure, which resulted in a poor carrier transport property of photo-generated carriers.

On the other hand, both SiH and SiH_2 absorption peaks were observed at 2000 and 2100 cm^{-1}, respectively, in the µc-Si:H:Cl films, were similar as to the µc-Si:H films fabricated using conventional rf and VHF PE-CVDs of SiH_4. No SiH at the surface of µc-Si phase was

observed. Moreover, the inclusion Cl in the microcrystalline Si network produces a new absorption band, which is assigned to Si-Cl bonds centered at 530cm^{-1} as described in ref. These suggest that film structure is a continuous Si network including a mixture of amorphous and crystalline Si phase, although the crystalline size is smaller. The film deposition rate reached 20 Å/s for the film synthesized from 5sccm SiH_2Cl_2, which was almost same as that for the film synthesized from SiH_4. Therefore, the fine structure of the μc-Si network from SiH_4 and SiH_2Cl_2 is different from each other.

The spectroscopy ellipsometry (SE) characterization was performed for the μc-Si:H:Cl films fabricated from a SiH_2Cl_2-H_2 mixture at different T_ss. Figure 17 shows the imaginary part of pseudo-dielectric function $\langle\varepsilon_2\rangle$ spectra of μc-Si:H:Cl films fabricated from a SiH_2Cl_2-H_2 mixture at different T_ss with that of μc-Si:H from SiH_4 with a thickness of 1 μm.

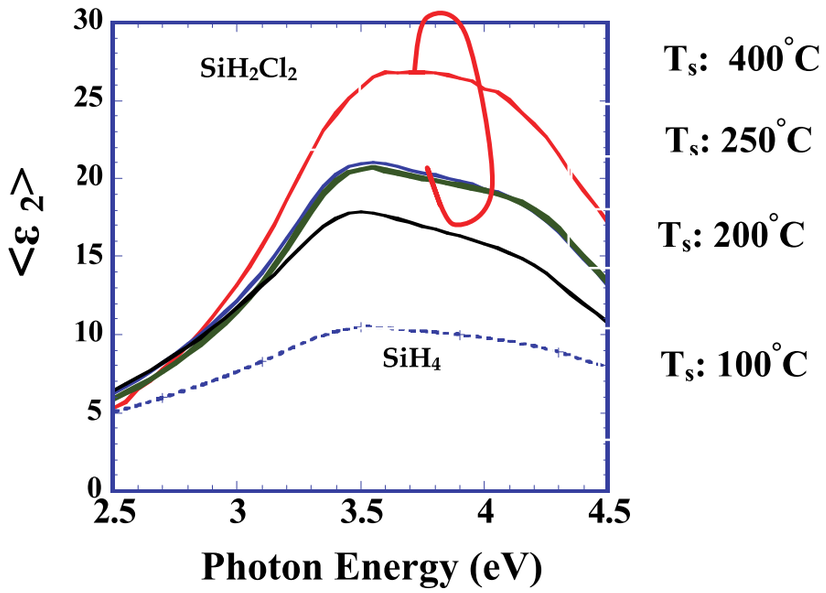

Fig. 18. Imaginary part of pseudodielectric function $\langle\varepsilon_2\rangle$ spectra of μc-Si:H:Cl films fabricated from a SiH_2Cl_2-H_2 mixture at different T_ss with that of μc-Si:H from SiH_4 with a thickness of 1 μm.

In both μc-Si:H:Cl and μc-Si:H films, the fine structures were observed clearly at 3.4 and 4.2 eV, which are attributed to the E_1 and E_2 optical band transitions, respectively, in the crystalline Si (c-Si) band structure. However, the magnitude of $\langle\varepsilon_2\rangle$ was much smaller in the μc-Si:H films from SiH_4 than in the μc-Si:H:Cl films from SiH_2Cl_2. Here, the magnitude of $\langle\varepsilon_2\rangle$ presents qualitatively the degrees of homogeneity and the surface roughness of μc-Si films.

The $\langle\varepsilon_2\rangle$ spectra were analyzed to understand the micro-structural properties of μc-Si:H:Cl films as described in section 3.2 above. The reflective index *n* at 2.2 eV determined by SE analysis also increased with T_s as determined using the reference poly-Si given by Jellison as shown in Fig. 19. It was higher for the μc-Si:H:Cl films in all T_s regions than that for μc-Si:H films. Thus, the rigidity of the Si-network is greater in the μc-Si:H:Cl films from SiH_2Cl_2 than in μc-Si:H films from SiH_4 using the high-density microwave plasma source.

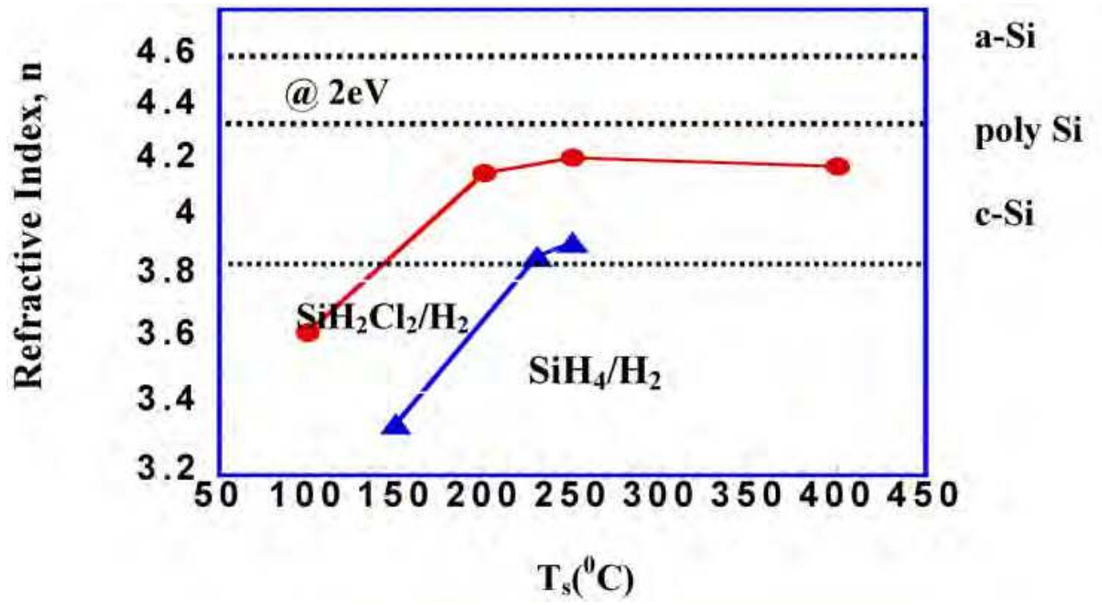

Fig. 19. The refractive index at 2.2eV in the bulk layer for μc-Si:H:Cl films plotted as a function of T_s

$f_{c\text{-}Si}$, $f_{a\text{-}Si}$ and f_{void} in the μc-Si:H:Cl films, corresponding to the bulk component, are shown in Fig.20 as a function of T_s together with those in the films synthesized from SiH_4 . Notably, f_{void} in the μc-Si:H:Cl films is less than 5% despite that being 10-15% in μc-Si:H.

The differences in the fine structure of the μc-Si network between μc-Si:H:Cl films and μc-Si:H films is shown in Fig.21. The degree of the excess dissociation of SiH_2Cl_2 is considered to be suppressed rather than that of SiH_4, because the threshold energy of SiH_2Cl_2 is higher than that of SiH_4, although the high energy part of electron energy distribution (EED) also depends on the feed gas. Film crystallization was promoted efficiently in the high-density and low-temperature microwave plasma of SiH_4. However, the resulting Si film structure was still porous with much f_{void}, although $f_{c\text{-}Si}$ was over 80%. These findings originated from the excessive dissociation of both SiH_4 and H_2 in the plasma, which promoted the generation rate of not only of SiH_3 but also short life-time radicals, i.e., SiH and Si. On the other hand, $f_{a\text{-}Si}$ was still more in the μc-Si:H:Cl films than in the μc-Si:H films with less f_{void}.

3.4 Defect density of microcrystalline silicon thin-film fabricated from SiH_2Cl_2 and SiH_4

In the case of MW SiH_4 plasma, film deposition rate 65 Å/s was achieved while maintaining the low defect density but that μc-Si:H film was not available for solar cell application because of film structure was porous as described above. Similar study was performed using SiH_2Cl_2 to realize the fast deposition of μc-Si:H:Cl films with no creating additional defects, higher flux of SiH_xCl_y generated by the primary reaction in the gas phase was supplied to the depleted growing surface by increasing flow rate of SiH_2Cl_2 at a constant pressure of 120 mTorr and T_s of 250˚C. Here, the deposition precursor SiH_xCl_y generated by the primary reaction in the plasma is expected to be supplied at the growing surface efficiently by increasing a flux of SiH_2Cl_2 at a constant pressure. Thus, the fast deposition of highly crystallized μc-Si:H:Cl film with lower defect density is expected because the efficient

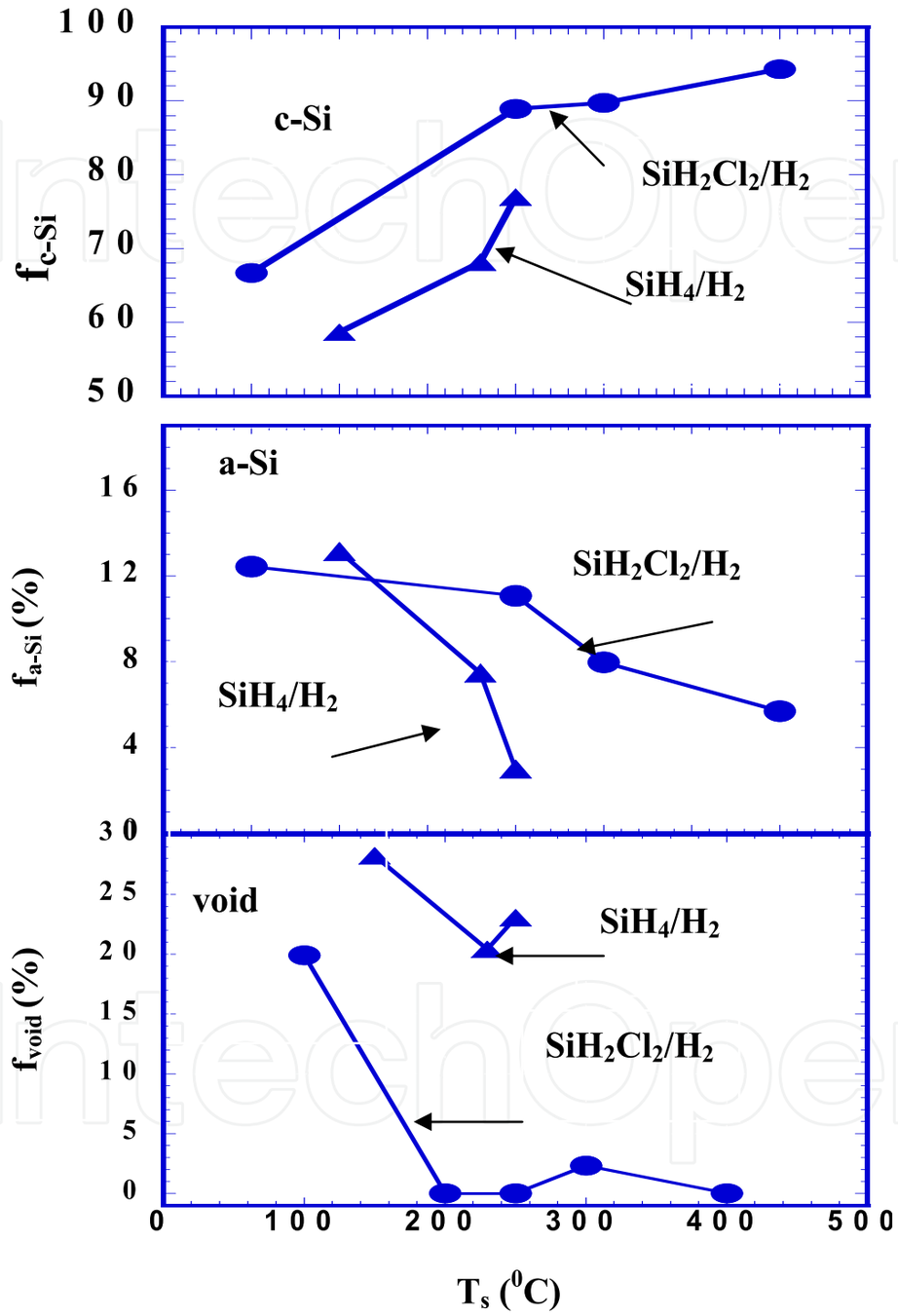

Fig. 20. The $f_{c\text{-}Si}$, $f_{a\text{-}Si}$, f_{voids} in the bulk (layer 3) of µc-Si:H:Cl films plotted as a function of T_ss. The results of µc-Si:H are also shown as a triangles symbol

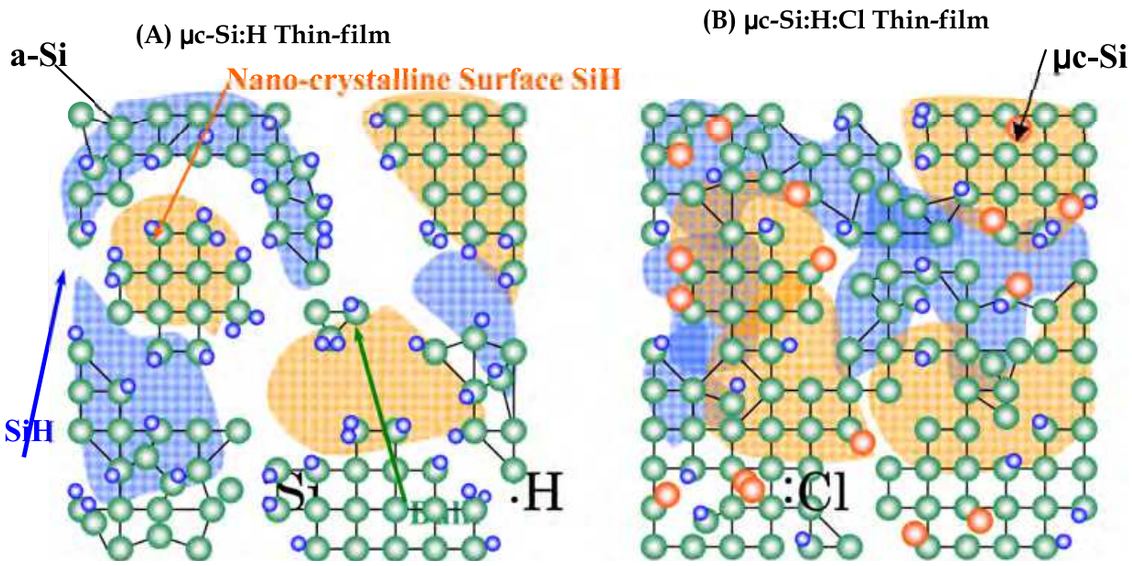

Fig. 21. Schematic of µc-Si:H and µc-Si:H:Cl network

termination of dangling bond by efficient supply of SiH_xCl_y is accelerated with the abstraction of H and Cl as HCl at the depleted growing surface. The deposition study was performed at two different T_ss of 250 and 400˚C. Figure 22 demonstrates N_ss and deposition rates of µc-Si:H:Cl films fabricated at different Fr(SiH_2Cl_2) at T_ss of 250 and 400˚C, respectively. The high deposition rate of 40 Å/s has been achieved with increasing Fr(SiH_2Cl_2) up to 20 sccm at T_ss of 400˚C and 250^{0}C respectively. The N_s was almost independent of Fr(SiH_2Cl_2) at T_s of 250˚C, whereas the N_s was markedly decreased at T_s of 400˚C. These are considered because of the efficient abstraction of H and Cl at the growing surface. The film crystallization was enhanced up to flow rate of 20 sccm of SiH_2Cl_2 at T_s of 400˚C. The N_ss were decreased systematically with increasing SiH_2Cl_2 at both T_ss to 4x10^{15} cm^{-3} at 15 sccm of SiH_2Cl_2.

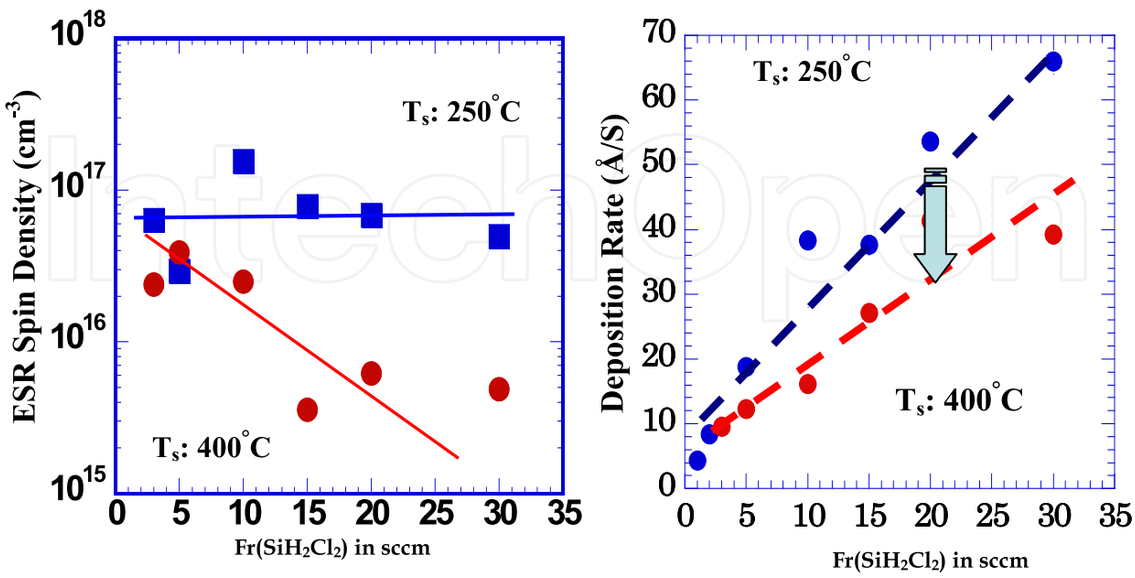

Fig. 22. ESR spin density and deposition rates of the µc-Si:H:Cl films fabricated at different flow rates of SiH_2Cl_2 at T_s of 250 and 400˚C.

By supplying the sufficient flux of SiH_xCl_y at a high T_s of 400˚C, the termination of dangling bond is accelerated with enhancing the abstraction of H and Cl. These findings are effective to form a rigid Si network with less void fractions. In fact, the defect density N_s was almost constant of 4-5×10^{16} cm^{-3} at T_s up to 250˚C, whereas it decreased markedly to 3-4x10^{15} cm^{-3} with Fr(SiH_2Cl_2) at T_s of 400˚C. Therefore, highly crystallized µc-Si:H:Cl film with low defect density was formed from a SiH_2Cl_2-H_2 mixture.

3.5 XRD and Raman spectra of microcrystalline silicon thin-film fabricated from SiH_2Cl_2 and SiH_4

The XRD diffraction patterns and the Raman spectrum of the µc-Si:H:Cl film fabricated at T_s of 250˚C and 400˚C with increasing SiH_2Cl_2 flow rates are shown in Fig 23 and Fig. 24. The XRD and Raman study of µc-Si:H:Cl films fabricated at T_s of 400˚C revealed that high film crystallinities with diffraction intensities ratio of $I_{(220)}/I_{(111)}$ of 1.5-8.75 and with Raman crystallinity of I_c/I_a:5-6 were obtained.

As a consequence, highly crystallized µc-Si:H:Cl film with low defect densities of 3-4x10^{15} cm^{-3} was fabricated at fast deposition rate of 27Å/s. These findings suggest that the efficient abstraction of H- and Cl- terminated growing surface.

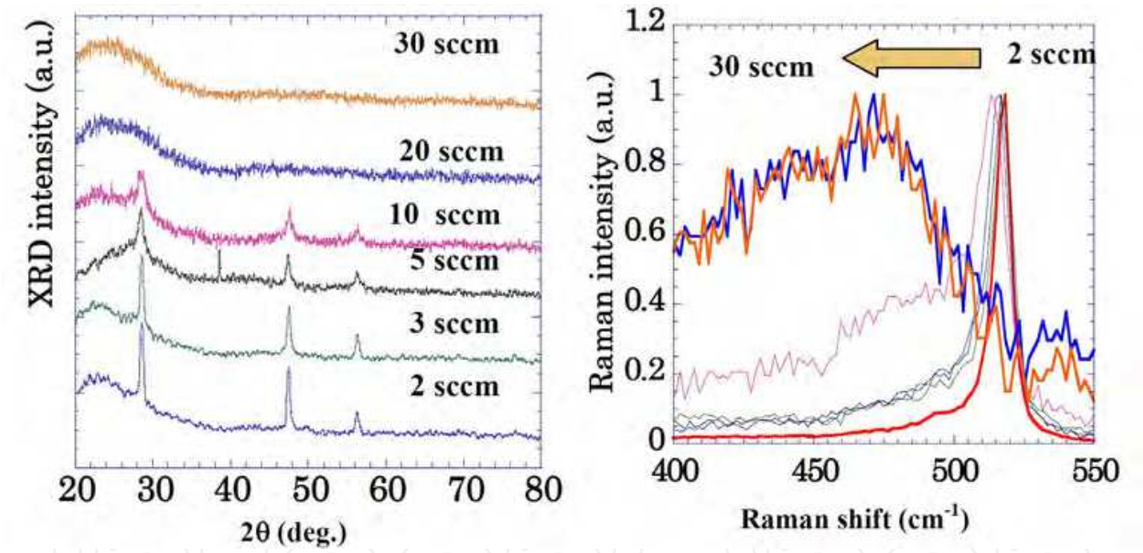

Fig. 23. XRD and Raman spectra of the µc-Si:H:Cl films fabricated at different flow rate of SiH_2Cl_2 at T_s of 250˚C.

3.6 Photoelectrical properties of a-Si:H:Cl and µc-Si:H:Cl films

Fig. 25 shows the relation between the dark and photo conductivities for the µc-Si:H:Cl films fabricated by increasing the SiH_2Cl_2 flow rate at the substrate temperatures of 250˚C and 400˚C. The photosensitivity reached at 5-6 orders of magnitude at room temperature. The level of photoconductivity was 10^{-5} S/cm under 100 mW/cm^2 white light exposure. The dark and photo-conductivities were the order of 10^{-12} and 10^{-5} S/cm, respectively, which shows highly photosensitive films. Fig.26 shows the activation energies for the µc-Si:H:Cl films fabricated by increasing the SiH_2Cl_2 flow rate at the substrate temperatures of 250˚C and 400˚C The activation energies of electrical conductivity were 0.40-0.80 eV, suggesting that both a-Si:H:Cl and µc-Si:H:Cl films were intrinsic semiconductor films.

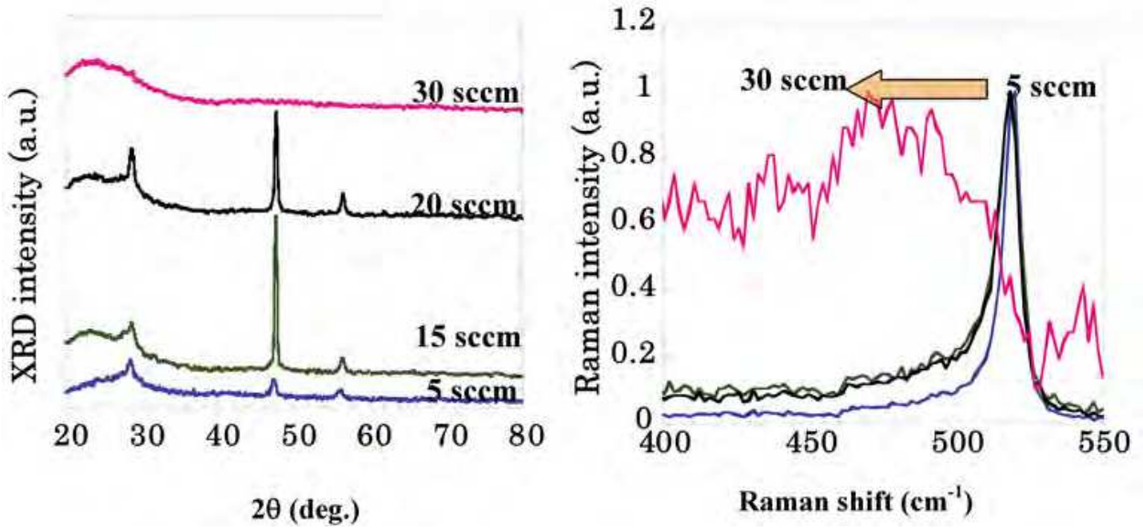

Fig. 24. XRD and Raman spectra of the µc-Si:H:Cl films fabricated at different flow rate of SiH_2Cl_2 at T_s of 250 and 400˚C.

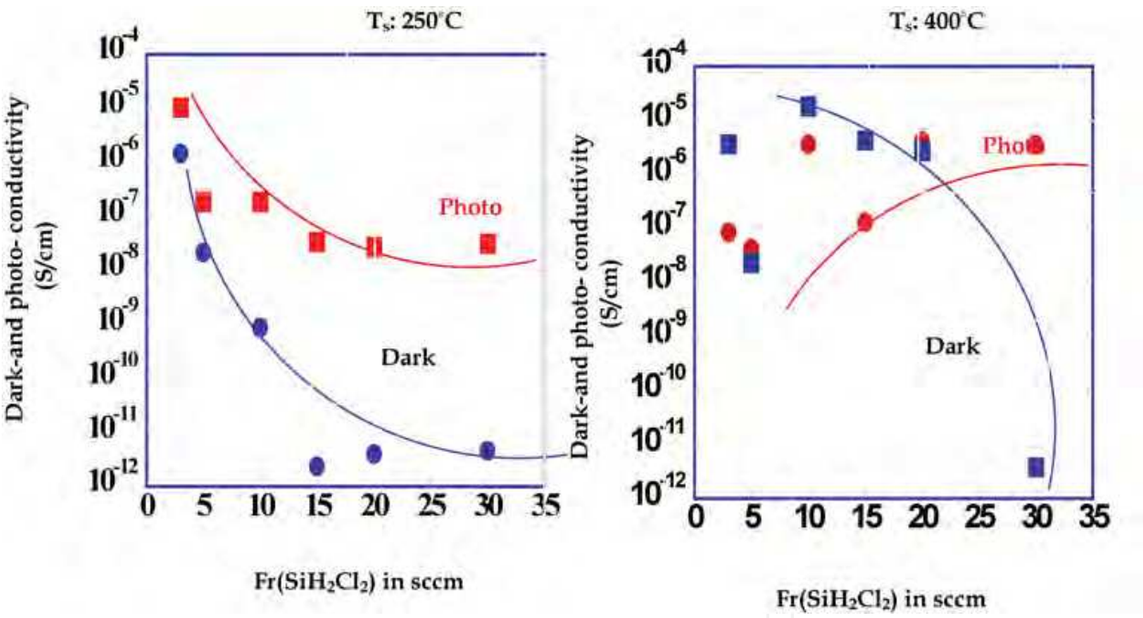

Fig. 25. Dark and photo conductivities for the µc-Si:H:Cl films as a function of SiH_2Cl_2 flow rate at the substrate temperatures of 250˚Cand 400˚C

4. Preliminary results of p-i-n structure µc-Si:H:Cl thin-film solar cells

The preliminary result of Si thin-film solar cells using µc-Si:H:Cl thin-film fabricated by the high-density microwave plasma (MWP) of a SiH_2Cl_2-H_2 mixture are shown here. High-rate grown µc-Si:H:Cl thin-films were applied to p-i-n structure Si thin-film solar cells as intrinsic absorption layer. The solar cell was fabricated using a single chamber system. The structure of the solar cell TCO/ZnO:Al/p-i-n/ZnO:Al/Ag is as shown in Fig. 27. After the

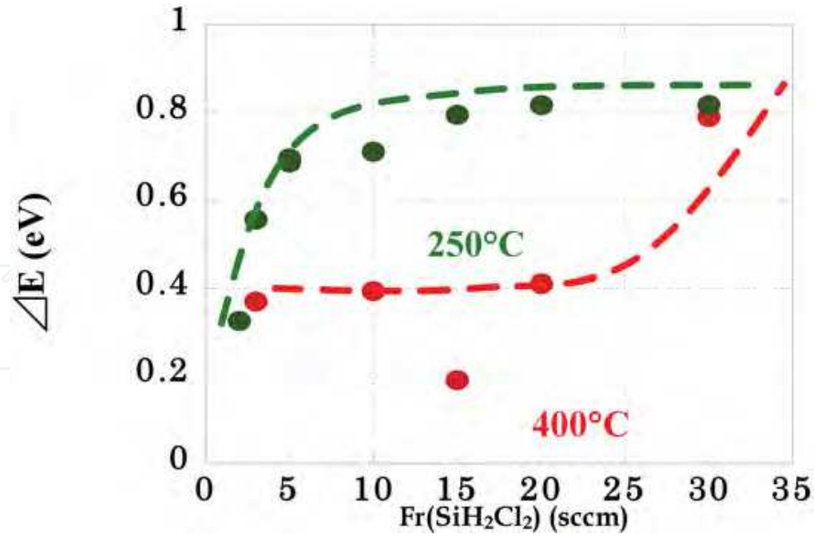

Fig. 26. Activation Energies, ⊿E for the μc-Si:H:Cl films as a function of SiH_2Cl_2 flow rate at the substrate temperatures of 250˚C and 400˚C.

deposition of ZnO:Al and p-type Si layers on SnO_2 coated glass, respectively by rf magnetron sputtering and plasma CVD methods, μc-Si:H:Cl film with a 2-μm-thickness is fabricated using a high-density microwave plasma as a photovoltaic layer and n-type Si layer was fabricated using conventional rf plasma CVD method. When the samples were being transported between the rf chamber and MWP chamber, they were exposed to air. Subsequently, ZnO:Al and Ag layers were deposited as a top electrode using a shadow mask with a 5×5 mm^2 holes. Table 3 shows the typical deposition conditions for p, i and n layers, respectively. Table 4 shows the typical deposition conditions for ZnO:Al, Ag layers fabricated by rf magnetron sputtering. The photocurrent-voltage, I-V characteristics under AM 1.5, 100mW/cm^2 exposure condition are measured and the performance of solar cell is characterized with open circuit voltage, V_{oc}, short circuit current, I_{sc}, fill factor, FF and conversion efficiency, η. The collection efficiency was also measured from 300 to 1200 nm under bias light conditions.

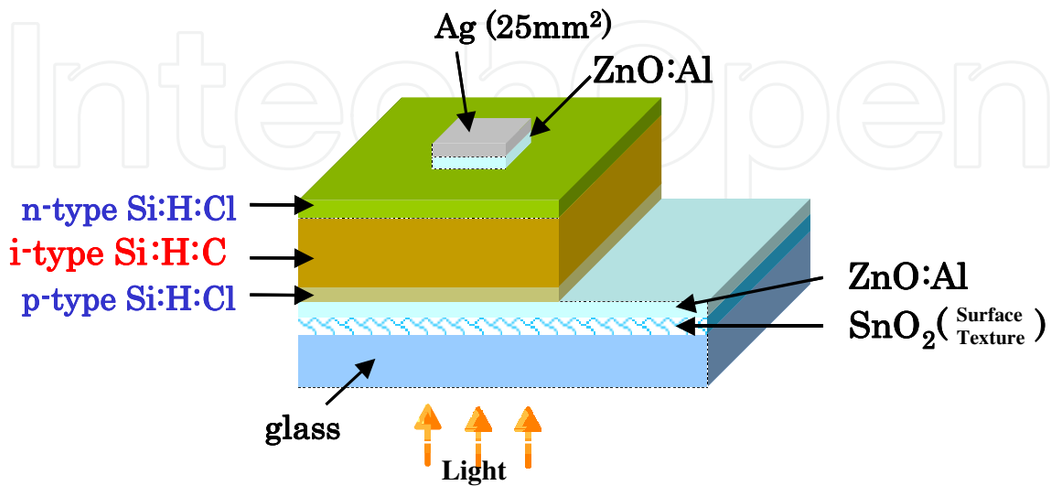

Fig. 27. The structure of the p-i-n solar cell

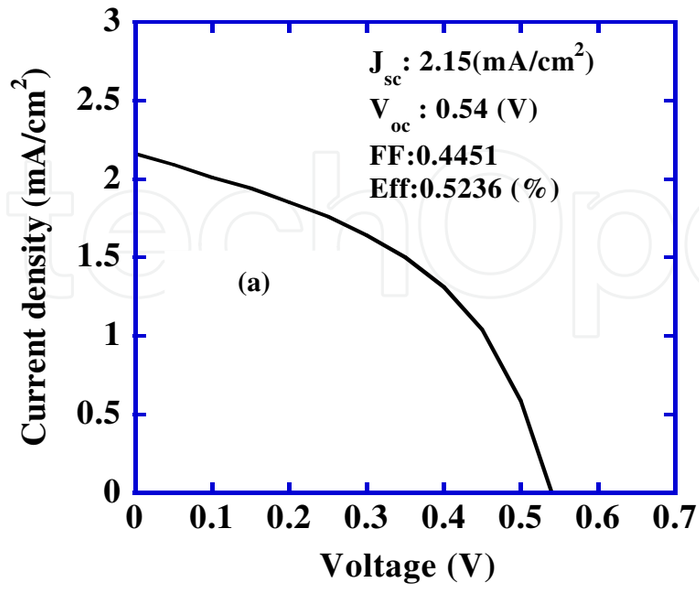

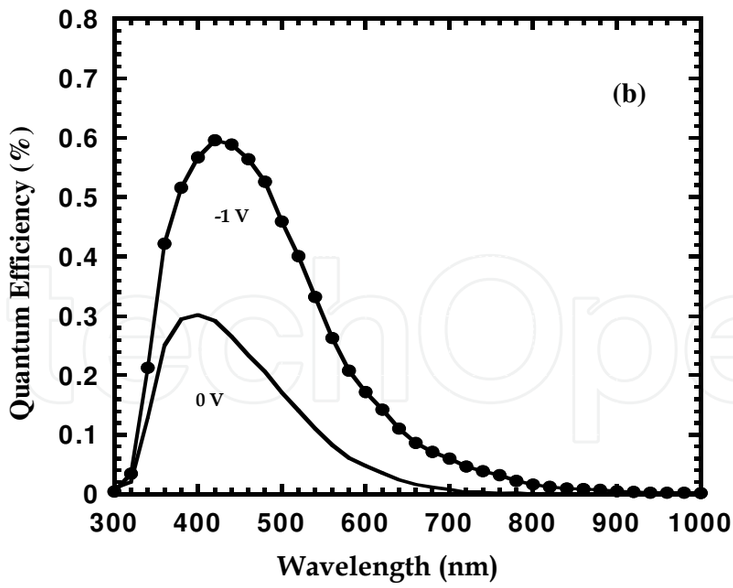

Fig. 28. (a) Photocurrent-voltage characteristics under AM 1.5 exposure condition and (b) QE spectra under -1V biased conditions of Si thin-film solar cells using a 1μm-thick μc-Si:H:Cl layer by high-density microwave plasma source.

	p(RF)	i(MW)	n(RF)
Substrate Distance (mm)	20	60	20
Substrate Temperature (°C)	250	250	250
Power (W)	5	700	5
Pressure (mTorr)	200	120	200
H_2 (sccm)	61	15	55
SiH_2Cl_2 (sccm)	3	3	3
PH_3 (sccm)			15
B_2H_6 (sccm)	9		

Table 3. Typical deposition conditions for p, i and n layers

	ZnO:Al(front side)	ZnO:Al(back side)	Ag
Substrate Position (cm)	6	6	6
Substrate Temperature (°C)	350	250	250
RF Power (W)	100	100	50
Pressure (Pa)	2.5	2.5	2.5
thickness (Å)	2500	2500	1500

Table 4. Typical deposition condition for ZnO:Al and Ag layers

Fig.28 illustrates photocurrent –voltage characteristics for Si:H:Cl thin-film solar cells under 100 mW/cm² white light exposure. Fig. 28a shows the I-V characteristics for the cell using µc-Si:H:Cl films fabricated at 20 Å/s by the high-density microwave plasma CVD of SiH_2Cl_2. The 5-6% efficiencies have been achieved for the cells fabricated by the conventional rf plasma-CVD method. However, the performance is still poor and the open circuit voltage, (Voc):0.54 V, short circuit density, (Jsc):2.15 mA/cm², Fill Factor, FF:0.5236 and the conversion efficiency was 0.5236% in the cell made by the high-density microwave plasma from SiH_2Cl_2 but solar cell performance is confirmed by the high-density microwave plasma from SiH_2Cl_2 for the first time. The diffusion of Boron and Chlorine happens easily in i-layer by the high-density microwave plasma. Moreover, the etching reaction of p layer has occurred because of the hydrogen plasma. It is required to evaluate not only a single film but it is also necessary to evaluate the each interface i.e. AZO/p, p/i and i/n in order to improve the solar cell performance. More over precise control of p/i, i/n, AZO/p interface formation is needed for obtaining the further high performance.

5. Conclusion

The highly photoconductive and crystallized µc-Si:H:Cl films with less volume fraction of void and defect density were synthesized using the high-density and low-temperature microwave plasma source of a SiH_2Cl_2-H_2 mixture rather than those from SiH_4 while maintaining a high deposition rate of 27 Å/s. The µc-Si:H:Cl film possesses a µc-Si and a-Si mixture structure with less volume fraction of voids. The role of chlorine in the growth of µc-Si:H:Cl films is the suppression of the excess film crystallization at the growing surface. H termination of growing surface is more effective to suppress the defect density rather than that of Cl termination. The fast deposition of the µc-Si:H:Cl film with low defect density of 3-4 $\times 10^{15}$ cm^{-3} is achieved with reducing Cl concentration during the film growth. Both a-Si:H:Cl and µc-Si:H:Cl films show

high photoconductivity of 10^{-5} S/cm under 100 mW/cm^{-2} exposure, are the possible materials for Si thin-film solar cells. The performance of p-i-n solar cell from μc-Si:H:Cl films using the high-density microwave plasma source was confirmed for the first time.

6. References

Ziegler, Y. (2001),More stable low gap a-Si:H layers deposited byPE-CVD at moderately high temperature with hydrogen dilution". *Solar Energy Materials & Solar Cells, 200*1. 66: p. 413- 419.

Graf S. (2005). "*Single-chamber process development of microcrystalline Silicon solar cells and high-rate deposited intrinsic layers*", in institute de Microtechnique, Universite de Neuchatel: Neuchatel.

Meillaud, F.(2005). "Light-induced degradation of thin-film microcrystalline silicon solar cells". in *31th IEEE Photovoltaic Specialist Conference*. 2005, Lake Buena Vista, FL, USA

Veprek, S. and V. Marecek (1968). "The preparation of thin layers of Ge and Si by chemical hydrogen plasma transport", *Solid State Electronics, 1968,* Vol. 11: p. 683-684.

LeComber, P.G. and W.E. Spear (1970). "*PECVD: plasma enhanced chemical vapor deposition*". *Physical Review Letters*, 1970. Vol. 25: p. 509.

A. Madan, S. R. Ovshinsky and E. Benn (1979). *Phil Mag*. B 40 (1979) 259

B. Chapman: Glow Discharge Processes. *Sputtering and Plasma Etching*, Chapter 9, John Wiley

A. Bogaerts, E. Neyts, R. Gijbels, J. van der Mullen(2002). *Spectrochimica Acta* B 57 (2002) 609J.K. Saha, N. Ohse, H. Kazu, Tomohiro Kobayshi and Hajime Shirai (2007). "18th *International Symposium on Plasma Chemistry proceedings*", Kyoto, Japan, Aug 26-31, 2007.

J. K. Saha, Naoyuki Ohse, Hamada Kazu, Tomohiro Kobayshi and Hajime Shirai (2007). *Japan Society of Applied Physics and Related Societies (the 54th Spring Meeting)*, Aoyama Gakuin University, March 27-March, 30,2007, 27p-M-2

S. Samukawa, V. M. Donnelly and M. V. Malyshev (2000). *Jpn. J. Appl. Phys*. 39 (2000) 1583

I. Ganachev and H. Sugai (2007). *Surface and Coating Technology* 174-175 (2003) 15.

J. K. Saha, H. Jia, N. Ohse and H. Shirai(2007). *Thin Solid Films* 515 (2007) 4098.

Y.Nasuno, M.Kondo and A. Matsuda (001). *Tech. Digest of PVSEC-12*. Jeju, Korea, 2001,791.

L. Guo, Y. Toyoshima, M.Kondo and A. Matsuda (1999). *Appl. Phys. Lett*. 75 (1999) 3515

G. E. Jellison, Jr. (1992). Opt. Mater. 1 (1992) 41

S. Kalem, R. Mostefaoui, J. Chevallier (1986). *Philos. Mag*. B 53 (1986) 509-513.

J.K. Saha, N. Ohse, K. Hamada, T. Kobayshi, H.Jia and H. Shirai (2010). *Solar Energy Materials & Solar Cells* 94 (2010) 524– 530.

J. K. Saha, N. Ohse, K. Hamada, K. Haruta, T.Kobayashi, T. Ishikawa, Y. Takemura and H. Shirai (2007). *Jpn. J. Appl. Phys*. 46 (2007) L696.

D.E. Aspnes (1976). Spectroscopic ellipsometry of solids, in: B.O. Seraphin (Ed.), *Optical Properties of Solids: New Developments*, North-Holland, Amsterdam, 1976, pp. 801–846 (Chapter 15).

Hiroyuki Fujiwara (2007). *Spectroscopic Ellipsometry: Principles and Applications*, John Wiley & Sons, Ltd., 2007, pp. 189–191.

H. Kokura and H. Sugai (2000). *Jpn. J. Appl. Phys*. 39 (2000) 2847

J. K. Saha, N. Ohse, K. Hamada, T.Kobayashi and H. Shirai(2007). *Tech. Digest of PVSEC-17.* Fukuoka, Japan, 2007, 6P-P5-68.

Y. Li, Y. Ikeda, T. Saito and H. Shirai (2006). *Thin Solid Films,* 511-512(2006) 46

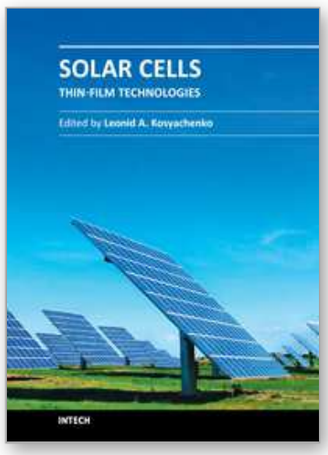

Solar Cells - Thin-Film Technologies

Edited by Prof. Leonid A. Kosyachenko

ISBN 978-953-307-570-9
Hard cover, 456 pages
Publisher InTech
Published online 02, November, 2011
Published in print edition November, 2011

The first book of this four-volume edition is dedicated to one of the most promising areas of photovoltaics, which has already reached a large-scale production of the second-generation thin-film solar modules and has resulted in building the powerful solar plants in several countries around the world. Thin-film technologies using direct-gap semiconductors such as CIGS and CdTe offer the lowest manufacturing costs and are becoming more prevalent in the industry allowing to improve manufacturability of the production at significantly larger scales than for wafer or ribbon Si modules. It is only a matter of time before thin films like CIGS and CdTe will replace wafer-based silicon solar cells as the dominant photovoltaic technology. Photoelectric efficiency of thin-film solar modules is still far from the theoretical limit. The scientific and technological problems of increasing this key parameter of the solar cell are discussed in several chapters of this volume.

InTech Europe
University Campus STeP Ri
Slavka Krautzeka 83/A
51000 Rijeka, Croatia
Phone: +385 (51) 770 447
Fax: +385 (51) 686 166
www.intechopen.com

InTech China
Unit 405, Office Block, Hotel Equatorial Shanghai
No.65, Yan An Road (West), Shanghai, 200040, China
中国上海市延安西路65号上海国际贵都大饭店办公楼405单元
Phone: +86-21-62489820
Fax: +86-21-62489821

IntechOpen